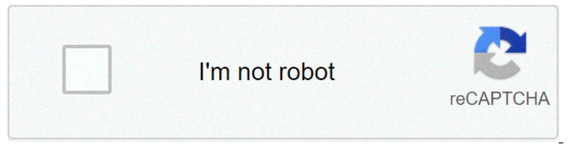

Continue

Allosteric regulation of acetyl coa carboxylase

structural base for the regulation of acetyl-co-teatro human carboxylase Acetil-Coa catalyzes the carboxylation of aqueousel-coa carboxylase, a limiting step of speed in fatty acid biosynthesis1,2. Acetyl-coa eukaryotic carboxylasis are large, multidimic homodimeric. acetyl-coa human carbosilase occurs in two isoforms: the metabolic, cytosolic acc1 and acc2, which is anchored to the external mitochondrial membrane and controls the fatty acid β-oxidation1,3. acc is regulated by a complex interaction of phosphorylation, binding of regulators and allosteric proteins and protein interactions, which is further linked to the formation of filaments1,4,5,6,7,8. These filaments have been discovered in vitro and in vivo 50 years ago7,9,10, but the structural base of polymerization and acc regulations remains unknown. here, we identify distinctly activated, separate and inhibited filament modules. we have obtained crio-electron microscopy structures of an active filament of an activated filament which is altered by the citrate (ACC-€ "citrate) and a form of inactive filament resulting from the bond of brct domains of the protein susceptibility of the type of breast cancer (brca1.) while non-mericac acc1 is highly dynamic, the formation of different filaments is blocked This unique mechanism of the enzymatic regulation through large-scale compliance variations observed in acc1 has potential or in the engineering of the switchable biosynthetic systems. the dissection of the regulation of acetil-coa carboxylase opens new paths towards the contract of upregulation of fatty acid biosynthesis in the disease. the acetyl-coa carboxylases of eukaryotics include the packaging of carboxylase biotin (bc,) the domains of biotin carblesyl carrier (bccp) and the carbossil transferase (ct,) as well as a domain of interaction (bt) and a region of the central domination not catalytic (cd,) that together bridge the bc and tc domains1 acetyl-coa carboxylation is a reaction in two stages: first, a biotin fraction connected bccp is carboxylated with atp consumption by the bc domain; Secondly, the resulting carbossybiotin is moved to the ct domain and the carbossy group is transferred to Acetil-CoA. in the acetyl-coa fungal carboxylase, the specific phosphorylation of the site in the cd regulates the activity by controlling the transition between an inactive, open state and an active, closed form, which is characterized by the dimerization of the domains BC11,12. human acc1 (fig. 1b) (hereinafter referred to as acc) is inactivated by phosphorylation to ser80, ser1201 and ser1216 by AMP-activated kinase protein (ampk) and ser78 and ser1201 by means of the chinase protein (pka;) the ser80 and ser1201 sites have the greatest impact on activity44. acc is further inhibited by its product Malyyl-CoA and derived Palmitoyl-Coa5 fatty acid. Citrate allostermic activator induces curing of acc in unsecured filaments up to 1 µm in length7; These filaments are the most active form of ACC6,7. Moreover, the tumor suppressor brca1 was hypothesized to regulate acc13. brca1 binds to acc through its tandem tandem brct domains14 (fig. 1a,) which recognizes ser1263 phosphorate in the cd of acc5. ser1263 is phosphorylate dependent on the cell cycle, presumably by a kinase13 based on cyclic-dependent13.15. brca1 binding prevents dephosphorylation of ser80 and thus inhibits activation of acc13. mutations in brct domains abolish binding brca1 by acc, resulting in high lipgenesis, which is a prerequisite for cell growth1: Organization of the domain and regulation of ACC.A, organization of the Domain of ACC and BRCA1; The color combination is used throughout the manuscript. SELECTED ACCS phosphosites are indicated. The BrCT domains of BRCA1 have been reported to interact with ACC via PSER1263. B, overview of the acc. Activation and polymerization are shown in green, inhibition in red and BRCA1 BRCA1 in blue. The binding protein of the Sterol regulatory elements (SREBP) controls the ACC expression; Other effects are the protein level. c, Specific Activity of ACC phosphorylated and dephosphorylated in the presence and absence of citrate. d, of the negative stain electron micrographs of three types of filaments ACC. Scale bar, 50 nm. and, ACC Activity in the presence of citrate and palmitoyl-CoA. Three individual measurements are shown for each condition in c and E.We ACC expressed in insect cells; mass spectrometry confirmed that the expressed protein has been phosphorylated on Ser80 (76%) and Ser1263 (94%). The defosforiolata protein has been obtained with the treatment Î »-fosfatasi, and it was five times more active of the phosphorylated protein (Fig. 1c). The addition of citrate to ACC dephosphorylated induces the formation of ACC-citrates filaments (Fig. 1d). Adding palmitoyl-CoA to preform filaments ACC-citrate in a molar excess of ten times, which is sufficient to inhibit ACC (Fig. 1e), induces a transition to another, filament form apparently correlated (ACC-citratepalm) (Fig. 1d). The BRCT ligation to phosphorylated ACC ACC produces a filament (ACC-BRCT) that has an architecture distinct from citrate or ACC-ACC-citratepalm filaments (Fig. 1d, Extended Data Fig. 1). The ACC filaments are highly flexible and form a mesh cluster on electron microscopy grids (Fig. 2a extended). Large projection provided samples suitable for cryo-electron microscopy (cryo-EM) studies of ACC-citrate filaments and ACC-BRCT. The helical symmetry was evident from raw images; however, the helical machining has not been applied due to the large repeat units and the pronounced curvature of the filaments. The monoparticella analysis gave the reconstructions at resolutions between 4.6 and 5.9 Ã Ã, as judged from the correlation of the Fourier shells (FSC, 0,143 threshold criterion) for different regions of filaments and filaments (Table 1 Extended Data, Fiji extended data. 2, 3). The quality of the map of subregions has been improved by using the post-map local symmetry (Fig. 4). With the exception of the BRCT and BC peripheral regions in the ACC-BRCT filament, all the elements of secondary structure were resolved clearly. The crystal structures of individual domains were mounted in cryo-EM maps. The dimeric BRCT domains were placed in an unambiguous manner on the basis of their interaction with phosphorylated (p) Ser1263, which is located on a flexible loop (amino acids 1257-1283) into the ACC CDC1 domain, despite the lower local resolution (Fig. 3c. extended). After the addition of citrate, the ACC defosforiolata assembles in 0.5-1 Î¼m filaments in length with a helical twist of about 120 ° and an increase of 154 Ã (Fig. 2a, b, Video Supplement 1). In cryo-EM maps, all domains, including the flexible carrier protein, are resolved. The filament is assembled for side stacking dimers ACC, which resemble the triangular conformation, closed previously observed for the ACC yeast (Fig. 2c): Two BC domains form a dimer, which has been recognized as a prerequisite for the BC12 Activity . The formation of filaments induced by citrates block then the ACC in an active conformation, which is not highly populated for ACC non-filamentous under conditions devoid of citrate (Fig. 5a extended) or ACC uncured residue under containment conditions citrates (Fig. 5b, 5c). Fig. 2: ACC-citrate struttura.a filament, ACC-citrate filaments (representation of the surface) are assembled from dimers ACC closed. Rise, twist, and width dimension ACC dimer are indicated. Left stranded with a dimer in the domain colors; right, colored filament domains. b, Top view of ACC-citrate filament. The elicoilici curls are marked with asterisks. C ... Dimer ACC ACC closed-citrate filaments shown with cryogenic map outline 0.0172. The yellow stars mark active sites. The domains of a protomaner are labeled. # The BCCP domain is positioned at the active carboxyl transfer site. A Citrate Dimer (Cardboard Rendering) is shown) With the Cryo-em map at the outline level 0.0158. The active sites of the carboxsy of carboxy and the bititers are marked with blue and red stars; The distance between the sites is indicated. BCCP connections are shown as daring tubes. The rotation of 120 Ã ° displacement of the BCCP to the BC domain is indicated. In the ACC two-phase reaction, the fraction of Biotin on BCCP is carboxylated from the BC domain and then closed on the CT domain. In particular, in the map cryo-em, BCCP is situated in an unambiguous position in the active site of Carbomsyl Transferase with BCCP connections alongside ordered (Fig. 2D), which firmly indicate that the CT domain acts as a Docking platform for BCCP in the Accompouring state, â‚¬ "citrate filaments. An additional dense is present for the fraction of biotin linked to BCCP (extended data fig.-5D - f). The active site of Biotin Carboxylase is located at 80 Ã - ... from the active site of carboxy transfer. A simple rotation of 120 ° of BCCP around hinges in the link linkers is sufficient to change its position between the two active sites (FIG.A 2D). DIMERATION INTERACTIONS- DIMERS IN ACC-â‚¬ "Citrate filaments are mediated by the CD. The CDN domain of ACC Molecule to contact CDLÃ ¢ â‚¬ "CDC1 molecule A + 1 and vice versa (fig. 2a, extended data fig. 6a). This interface is based on the docking of a cycle between propellers nî ± 4 and nî ± 5 of CDN in a cot formed by strand Î²1 of the CDC1 sheet Î²1 and Helice Iî ± 2 and the cdl ± 4 (extended data fig. 6aÃ ¢ â‚¬ "C). The patches involved in this interface are highly preserved between the metazoa, consistent with previous observations of Avian, Murine and Bovine Acc7.16 polymers. However, they are less preserved for ACC Fungal (extended data Fig. 6D). Overlapping of the structure of Saccharomyces cerevisiae acc (Scacc, IDD ID ID: 5csl) In fact it suggests that the yeast enzyme is incompatible with the observed mode of filament formation (extended data fig. 6B, C). It cannot be excluded, however, that the flexibility of the regions of the cycle involved or the slight variations of the helical symmetry can allow the ACC polymerization in mushrooms. To our awareness, no polymer forms of purified mushrooms have been reported. Two recent studies have displayed Fungal Acc in vivo in elongated focali using a large field or confocal 17.18 microscopy, however, they have not provided further tests for the direct polymerization of acc.The acc-acc-acc Citrate filament. Select for a dimeric BC arrangement, even if the BC domains are not directly involved in the filament assembly. The conformative restriction of the CD is apparently sufficient to stabilize the dimerization of the BC domain. However, the Dimfer interfaces of the disturbed BC domain, for example, in response to the Ser80 phosphorylation, as previously proposed12, could still be compatible with this form of a filament (extended data fig.- 1). Addition of a further excess of soft feedback COA feedback inhibitor reduces ACC activity activated by citrate by about 60% (fig.Ã ¢ 1E). Also deactivates the architecture of the preformed acc Citrate filaments, resulting in the other form of filament, which we have defined acc-â‚¬ "citratapalm (fig.Ã ¢ 1d). Acc-â‚¬" citrateepalm forms a few minutes from ACCÃ ¢ â‚¬ "citrate and is stable for several hours. Acc-â‚¬" CitratePalm filaments begin to dissociate only at concentrations of palmitoyl-coa considerably higher, possibly due to palmitoyl-coa that acts as a detergent (extended data fig. 7a). In acc-â‚¬ "citratapalm, the helical spine is thinned and the globular satellites flank the sides of the filaments. Suppose that the two forms of filament are correlated and that the interpreteromeric spine of acc5 â‚¬" citrate is present also in acc-â‚¬ "citratapalm. The most likely candidate for globular satellites is the BC domain, which is Observed in dimeric and monomeric forms as part of the ACC15 fungal or aspirated by human ACC220 and is not part of the spindle spine. We hypothesize that the tie of Palmitoyl-COA leads to changes in conformity, possibly on the CD or in the Domain BC Dimer interface, with consequent consequent DIMER Destabilization BC (extended extended data and, therefore, reduced activity. Upon catalytic bond of the BRCT domains, phosphorate forms ACC-stranded two filaments with triangular section and, for each trefol, a helical torsion of about 120 ° and an increase of 190a A (Fig. Ã 3AA ce additional Videoa 2). Each Strand assembly from open Z-shaped ACC dimers that are aligned along the filament axis (Fig.A 3d). Dimerica BRCT of domains sideways decorate the filament (Fig.A 3b) and Interlink dimeri ACC adjacent. The filament is composed of nodes of dense protein interconnected by arm-like ledges (Extended Data Fig.A 7câ e). Because of the Z-forma elongated, each contributes three consecutive nodes, and each node is composed of two CT domains of a molecule, one copy each of the CDC1, CDL, CDN, BT, BCCP and BC of B and BA 1 molecules, as well as a BRCT domain interconnection CDC1 of B and BA 1 molecules (Fig.A 4a extended, Fig. The connection arms are made of cdc2 domains (Extended Data Fig.a 7e), which contact the CDN and CDC1 domains of the same PROTOMERO in a node and the CT domain in the previous node with interface zones of 430A A 2, A 2 870A and 450 A 2, respectively. Fig. 3: Acca BRCT filament structure.A, The two filaments Acca BRCT (surface representation) are shown in blue and yellow, respectively. Climb and rotate for a wire, width and ACC dimer size are indicated. b, The BRCT dimer (corral, indicated) is placed at the periphery of the filament. The strand is shown in grey with an ACC dimer colored by domains. c, Filament seen from the top illustrating the triangular shape and central positioning of the Î ± -helical curling. helical torsion is indicated. d, Inverse Z-shaped ACC dimer shown with crioconservates EM map. Yellow stars mark active sites. Domains a PROTOMERO are indicated. Map boundary level (0.007) was chosen to reveal the density of all domains. Fig. 4: inter and intra-strand interactions Acca BRCT filaments.a, superior, Acca BRCT filament with protomers from two labeled filaments and indicated section plane. Half, section reveals connection of the CDN four propeller bundle to the -helical Î ± extension and the curling as the main inter-filament interaction. An example of each domain is labeled, colored contours indicate the PROTOMERO connectivity. Lower, enlarged view (rotato) of the interaction zone. b, Top, Tap BRCT filament with protomers from a wire labeled. Center and bottom, view larger than the CDC1â BRCT interaction. Each dimeric BRCTs PROTOMERO binds to a phosphosite loop. Contours show connectivity, the dotted lines indicate unshaped residues. The phosphosite cycle is shown in bold. Extended data shows Fig.a 7g further enlarged view.the inter-strand interactions are formed in the center of nodes, in which you make four helix of the Î± CDN-helical domains from molecules B and BA 1 form an interface of about 900A A 2 with the Î C-terminal ± -helical curling and the previous Î± extensions -helical of the domain TC A molecule (Fig.A 4a). The helical helical helid had previously been linked only to the stabilization of the CT and binding21 compound dimer, but apparently it has a central role in the organization of the Acca BRCT filament. The 85 C-terminal amino acids of the CT domain are in fact highly preserved among other ACC mammals with 52A 75% sequence identity in human couples and, while the C-terminal sequence identity of the CT domain in ACC yeast is only 13% 21. The four-helix bundle of the CDN domain is involved in both the inter-Strand interactions in Acca BRCT filaments and the dimer interconnected interfaces of Acca Citrato. The BC domain in Acca BRCT is monomeric, so Acca BRCT filaments are a form of inhibited ACC11,12,19. Within a node (Fig.A 4a), the distance between the active sites of BC domainsB and BA 1 is 143a Ã and the distance to the site active in the CT domain of a molecule is only 70a Ã, lower than theDistance in the ACC-citrate active filament. However, even if the BCCP domains were in a catalytically competent state despite being monomeric, the BCCP domains would be sterically able to reach one of the active sites. The inverse Z-Shape of Dimeri ACC in ACC-BRCT is an intermediate between the open and inactive conformation of the thermophilic chaetomium11 and the yeast Acc22 and the closed and active form of the non-polymeric yeast ACC or of the human filaments acc-citrate (Extended DATE Fig. 8a) The distinct conformations of the Human ACC dimers derive from the decline in the hinges on the CD (fig. 8B-D) in ACC-BRCT, the BC domain is located so that its B-Domain cap resides in the CDN A domain a Shape of C (Extended Data Fig. 8E) with greater conformational variability, based on the quality of the map. In particular, the positions of the BT and BCCP domains related to CDN are largely stored between acc-citrate and ACC-BRCT (Fig. 8F), however, the BCCP domain in ACC-BRCT, similar to the BC domain, is more flexible and not moored at the active carboxyl transfer site as in acc-citrate (Fig. 2D, Extended Data Fig.). Intra-strand connections in ACC-BRCT are mediated by CDC1 domains of successive ACC molecules. These domains only form a minimum contact area of 100 Ã ... 2. The ACC-BRCT filaments are not observed in the absence of the BrCT domains (Fig. 1,) indicating that the CDC1 contact is not enough to independently establish the polymerization Stable (fig. 4b) The CDC1 domain includes the phosphorus loop (amino acids 1257-1283), which is messy in the crystalline structure of the ACC11 BT-CD region and contains the PSER1263 controller. The phosphoritic cycle provides the binding site for BrCT, as previously demonstrated in the structure of a monophorated peptide mimic (1258-DSPPQ-PS-PTFPEAGH-1271) linked to monomeric BrCT15. In ACC-BRCT, however, a SCRT Domain Dimension binds to the phosphor (partially disordered) loops of subsequent acc acc CDC1 in a single filament. The BrCT domains interact with an interface area of about 800 Ã ... 2 in the Dimero BrCT, which takes place mainly with the interactions with protruding phosphorus loops (Fig. 4B, Extended Data Fig. 7F, g,) and only marginally contact The core of Filamento ACC (interface area of about 100 Ã ... 2.) An equivalent mode of Protein Simerization has been observed with the Peptides of the ABRAXAS protein: the single-piece Abras peptides interact with the monomeric BrCT, while i Peptides containing a second pser preceding the first form of dimeric bosphosite brttâ € "complex23 phosphopeptide. In ACC, Ser1259 precedes the PSER1263 canon recognition site of BrCT. The phosphorylation of the ser1259-equivalent residue was observed in vivo in the Topo Acc24, and Ser1259 is also partially phosphory in the human cell-expressed insect used here. Size-exclusion chromatography Coupled to the scattering of Multi-angle laser light in the presence of monofosphorylato (1255-CFSDSPPQ-PS-PTFPEAG-1270) and phosphorylated (1255-CFSD-PS-PPQ-PS-PTFPEAG-1270) The Peptides ACC provide support tests for a Sliver complex BRCT-SPO (extended figure fig. 8h) This propensity for the formation of dimensions complexes allows StraCt to act as a molecular clamp to interconnect the ACC dims in ACC-BRCT and explains addiction of training of this type of filament on BrCT. The interaction with the full length BRCA1 inhibits PSER80 defosurelation in ACC13. This effect is not explained directly by the Straight Slimming bond, which contains only 213 of the 1863 amino acids in BRCA1. However, the minimum distance between BrCTs and the BC domains containing PSER80 in ACC-BRCT is only 40. Crio-em reconstructions reveal how ACC activity is regulated by the formation of filament types Although the cytrate's tie itself cannot be displayed at the current resolution. Non-meric ACC dimeri catalystically competent and incompetent states. Citrate blocks ACC in a catalytically competent state by inducing the formation of ACC-citrate filaments (Fig. 5). In particular, the non-polymerized ACC yeast is also regulated by conformational closure: phosphorylation to Ser1157 and subsequent link of pSer1157 to a positively charged slot in the formation of active dimer CD defavors, closed 11,12,22. Citrate binding in human ACC may also exert its effect through the CD, although binding to the BC domain dimer interface was also previously suggested25. The palmitoyl-CoA inhibitor modifies the filaments induced by the citrates, presumably resulting in reversible release of the dimerization of the BC domain. AMPK-mediated Ser80 phosphorylation was also proposed to disturb BC dimerization domains12,22. Fig. 5: ACC polymerization integrates regulatory signals. AMPK Ser80 dimeric ACC phosphorized in response to the state of cellular energy, while Ser1263 is phosphorized depending on the cell cycle. At the time of the citrate bond, ACC with Ser80 non phosphorylated form activated filaments ACC-citrate with dimeric BC domains. ACC produces malonyl-CoA for fatty acid biosynthesis. Palmitoyl-CoA feedback inhibitor modifies ACC-citrate filaments, potentially interrupting the dimerization of the BC domain. The BRCT domination binding of BRCA1 to pSer1263 involves the formation of inactive ACC-BRCT filaments with monomeric BC domains. The gray circles show an enlarged vision of the BC organization. The BRCA1 binding at full length inhibits the dephosphorylation of pSer80 and pSer1263. BRCA1 has been involved in the regulation of the cell cycle-dependent of biosynthesis and fat-acids in adipose tissue by the interaction with ACC13. Our results extend the previous work on the interaction of cytosolic ACC with BRCT domains of BRCA1, which is mainly located at the core, but also occurs in cytosol26. The interaction of BRCT dimming domains with ACC phosphorus loop induces the polymerization of open and extended ACC dimers in double filament ACC-BRCT filaments with a distinct CD conformation and monomeric BC domains (Fig. 5). BRCA1 was reported to keep ACC in an inactive state by preventing the dephosphorylation of pSer8027. In the ACC-BRCT filament, the corresponding interaction could not be displayed, but can nevertheless be explained by the resulting proximity of BRCA1 to a Ser80 exposed in the monomeric BC domain. Further studies will be necessary to confirm and define the live interaction of ACC and BRCA1 and the consequences for the regulation of both proteins. ACC is a textbook example of the formation of metabolic enzyme regulator filaments28. ACC has a central role in primary metabolism; its upregulation is linked to obesity-related diseases1,29,30 and tumor growth31,32,33. Fungal ACC is also a polyketide A19 soraphen antifungal target. Identifying distinct interactions in ACC filaments our data also provide a structural basis to manipulate the ACC polymerization in vitro and in vivo, for example, for therapeutic intervention against ACC overactivation. The coding sequence for ACC1 (amino acids 1–2346, Genebank #Q13085) was cloned in a modified pACEBACI expression vector (Geneva Biotech) containing a Gateway (LifeTechnologies) cassette with a N-terminal His10–Myc–FLAG tag according to the manufacturer's instructions. The generation of bacteria and viruses was carried out in Sf21 (Expression Systems) cells in Insect-Xpress medium (Lonza), following the MultiBac instructions. No micoplasma contamination was detected using MycoAlert detection kit(Lonza), no identification of cell lines has been made. The cells were collected three days after centrifugal infection and stored at −80 °C until further use. Cellular pellets have been dissolved in the buffer of lisisM TRIS-HCL PH 8.0, 150 mm NACL, 40 mm Imidazole, 2.5 mm MGCL2, 5% glycerol, 5 mm Î²-Mercaptoethanol (Î²-ME)) With the addition of a spatula tip of DNASEI, LYSED from Sonication and the LYSATE was eliminated by ultracentrifugation. The soluble protein was purified by the chromatography of immobilized metal information using the Ni-Charged resin (GENSCRIPT, NI-IMAC). After the elution from the Ni-iMac, the buffer has been mistaken for the gel filtration buffer (20 mm Bicine pH 8, 150 mm NACL, 5% Glycerol, 5 mm TCEP) using a SephaDEX G-25 column (GE Healthcare). To guarantee the highest levels of Biotinylation, ACC has been biotinylated in vitro during the night in a reaction containing 50 mm TRIS-HCL, pH 8.0, 16 mm BICINE PH 8, 5.5 mm MGCL2, 180 mm NACL, 3 mm ATP, 14% Glycerol, 4 mm TCEP, 0.5 m biotin and 3.7 Î¼m Bira. The degree of Biotinylation was evaluated by Shift gel on streptavidine binding (Fig. 5D extended); 0.5 Î¼g ACC has been incubated to ratings of 2: 1, 1: 1, 1: 2 and 1: 5 with Streptavidin (Sigma) for 30 min at room temperature. The samples were analyzed by SDS-page using a mini-protean TGXTM Precast Gel (Biorad) of 4-15%. The buffer has been exchanged again, and ACC has been concentrated using a mass centrifugal concentrator of 100,000 pieces (Amicon) and polished with dimension-exclusion chromatography (superose 6, GE Healthcare). The Defosphorylated ACC was obtained after nocturnal incubation with phosphatase Î »-protein (New England Biolabs) before the last gel filtration pass. The removal of phosphoryl groups on the completion of 92% was confirmed by mass spectrometry. Purified ACC was concentrated at 4 mg / ml and 2.7 mg / ml for phosphorylated and defosphorlated proteins, respectively, in the gel filtration buffer. Coding sequences for the BrCT domains of Human BRCA1 (Genebank adhesion # BC115037), delivered in vector PCR-Bluntii-mouse, were under-cloned in PETG-10A (EMBL) and expressed in Arab-inducible one shot BL21-AI Escherichia coli (thermofisher, C607003) overnight at 16 Ã ° C. The cells were collected, loose in the Lisi buffer (50 mm Tris-HCL pH 8.5, 150 mm NACL, 25 mm imidazole, 2 mm MGCL2, 5% glycerol, 5 mm Î²-ME) and lysed from sonication. The protein was purified by Ni-IMAC and chromatography with the exclusion of the dimensions (Superdex200, GE Healthcare) and concentrated at 7.8 mg / ml in the acc. The proteins were stored at 80 ° C after freezing the flash in liquid nitrogen. ACC Polymerization and Electron Microscopy of negative stain The small MIG12 protein modifier has been reported to be involved in the formation of the ACC16 filament, however in our in vitro experiments with purified components, the presence of MIG12 has not been necessary for the formation of ACC -Critat or other forms of filament. To form acc-citrate filaments, DEFOSFORYED ACC was dialyed overnight against 50 mm HEPES / KOH pH 7.5, 10 mm K3Citrate, 0.1 mm EDTA, 5 mm Î²-ME and diluted at 20â € "40 Î¼g / ml in the same Buffer without Î²-Me. The same treatment was applied to phosphorylated protein, which produced aberrant filaments and rings (fig. 1). In order to obtain acc-brct filaments, a phosphorylated acc accia has been mixed with an excess to overtime high times of BrCT domains and engraving at room temperature for 1 h, before dilution using 25 Î¼g / ml gel filtration buffer. The same treatment was applied to the defosphorized protein, which did not lead to filament formation (fig. 1). For acc-citratepalm filaments, acc-citrate was prepared and palmitoyl-coa was added to excess molar ten times more. The phosphorylated and defosphorylated acc acces diluted using the gel filtration buffer at 25-40 Î¼g / ml to obtain the samples of the protomaner acc. All negative stain grids have been prepared applying 5 Î¼L Protein solution with 200-mesh carbon copper grids (prepared at home). The sample was allowed to adsorb for 5 s. Subsequently, the grids were washed three times with the corresponding buffer and once with water, before two rounds of coloring using the 2% of Uranil acetate for 5s and 20s, respectively. Negative negative watertight They were acquired on a philips cm-100 tempmool at a nominal magnification of 92,000 .. bicustropy electron electron microscopy collection and protomeri management programs of human acc acces were prepared as described above and imagined on a fei 200 kv talos fitted Of a FEI CETA CMOS Camera Pixel 16m. The data was collected at a nominal magnification of 73,000-, resulting in pixel format of 2.01 Ã £ .... The contrast transfer function (CTF) was estimated using GCTF34 from 251 images collected. The particles (22.005) were collected semi-automatically using the boxer implemented in EMAN235. The 2D iterative classification has been carried out using Relion36 to produce class 2D medium containing 9,920 particles. ACC grids, acc Citrate filaments were prepared as described above and were imagined on a FEI 200 kV talos TEI talos equipped with a CMOS camera of FEI CETA 16M pixels. The data was collected at a nominal magnification of 57,000-, resulting in pixel format of 2.59 Ã £ .... CTF was estimated using GCTF from 702 images collected. The particles (14.392) were manually collected using Relion. The 2D iterative classification has been carried out using CRYOSPARC37 to produce 2D class averages composed of 2,379 particles.cryo-em grid preparation preparation and free data for acc-â‚¬ "citrate filaments, Defosforilated acca has been dialysis during the night against 50 mm Hepes / Koh pH 7.5, 10 mm K3citrate, 0.1 mm EDTA, 5mm Î²-ME. For initial grids, the protein was diluted at 300 Î¼g / ml using the same swab without Î²- Me, and Lacey's Grills (in Cu 300 Mesh Carbon, Ted Pella) have been prepared using a FEI Vitrobot IV brand (4 3s blotting time) with 4 Î¼l sample. The optimized grids have been prepared as described above, However, the protein was diluted at 400 Î¼g / ml; N-Dodecil-Î²-D-maltoside was added to 17 Î¼m and the mixture was incubated for 1 hour at room temperature. To get acc-â, ¬ "BRCC filaments, phosphorylated acc (4 mg / ml) have been mixed with an excess molar for eight times D The BrCTs and dialysis against the gel filtration buffer without glycerol. The filaments were diluted at 0.75 mg / ml directly before applying to the grids. Lacey's grids (in Cu 300 Mesh carbon, Ted Pella) were prepared using a FEI Vitrobot IV brand (4 Ã ° C, 3.5s of stain time). The samples were imagined using a Titan Krios FEI equipped with a Gatan image filter (Quantum- Ls GIF, 20V filter for zero loss) and a direct electron detector of Post-GIF K2 (Gatan). The images were recorded at 300 kV with a nominal magnification of 130,000- in super resolution mode with a pixel size of 0.529 Ã £ ... for pixel super resolution on the sample level, applying a defocus interval of Ã,,1 Î¼m to â, '2.5 Î¼m for Citrate and Ã ¢' 1 to Ã ¢ '3.5 Î¼m for ACCÃ ¢ â‚¬ "BrCT in dose fractionation mode. For ACC, citrate filaments, 40 frames, to ~ 1, ... Ã, '2 per frame (yielding a total dose of 40 and ... Ã ¢' 2) were recorded; For ACCÃ ¢ â‚¬ "Stralamps Filaments 80 frames, at ~ 1, ... Ã,2 per frame with a total dose of 80 and ... Ã ¢ '2 were recorded. Imagine processing for acc-â, ¬ "Citrate filaments, 13.671 films were recorded using Serialem38. The recorded films were pre-processed online with focus39. The films were cut out by Fourier from 8K to 4K, with consequent effective size of the effective pixel of 1.058. CTF was estimated using CTFFind4.141. The low quality micrographs have been rejected by the estimate of the resolution of the CTF (> 10 âƒ ...), of the sample drift (> 80. On fire. The particles (247.337) were stored manually using Relion 2.0.3 from 13.671 micrographs42 and all further processing steps were conducted in Relion 2.1B1, unless otherwise mentioned (extended data fig. 2). The 2D classification was performed using CRYOSPARC and the 174.224 resulting particles were used for an AB-initio reconstruction. This volume was then used as a starting template for 3D Relion classification. The volume of the class "With the highest population was used for the positioning of Crystal Domain structures ACC (BC, PDB ID: 2yl2; CD, 5i8711; CT, 4ASI) and subsequent creation of mask. A masked masked 3D It was executed and the two classes with the highest population were selected for a 3D refinement focused on 147.822 particles that produce a map at the resolution of 6.6 ×. The film, particle polishing and the subsequent additional 3D classification produced a population of 131.062 particles, which were used for a final focused 3D refinement. The post processing produced a map at 5.4 × Resolution judged by FSC using the 0.14343 threshold criterion. The local resolution was determined by RESMAP using half-mapping reconstruction44. Application of Global C2 symmetry during reconstruction did not greatly improve the quality or resolution of the general map. For ACC-€ "The BRCT filaments, were recorded 3,233 films, aligned and correct for the movement induced by the beam using Motioncor240 (extended data fig. 6). The micrographs of poor quality were rejected by the estimate of the CTF resolution (GCTF34,> 6 Ã ...), derived from the sample (> 80 Ã ...) and defocus values (â'3.5). The particles were semi-automatically boxing using Relion 2.0.1 and all further processing steps were conducted in Relion 2.0.1, unless mentioned (extended data fig.8 3). The unsupervised 2D classification was performed using 67.903 particles from 2.924 micrographs and particles that did not contribute to high-resolution class mediums were excluded from further refinement steps. An initial model was created using E2initialModel.py implemented in EMAN235, filtered at 50 ã ... and used for 3D classification in four classes. The particles of the two classes with the highest population (44.997) were used for 3D sophistication, producing a map at 9,7 × ... The quality of the map was greatly increased during post-processing and refinement of the film at 7.7 × ... This map was used to unebrokenly hook the individual crystal structures listed above, producing a first model used to create two masks. The first mask contained the main particle consisting of CT, CD and BT domains. The second mask contained four complete knots. The particles have been re-classified with C2 attribute symmetry and a focusing refinement using the main mask produced a map at 6.6 Ã .... After processing the post using the two different masks and cinematic refinement, the resolution of maps was increased to 4,6 × and 5,9 Ã ..., respectively, based on the FSC 0.1434343 threshold criterion. The local resolution was determined by Resmap using half-map reconstructions44. Model building and refinement of the highest resolution maps of both filaments, ACC and BRCA1 BRCT crystal structures (PDB ID: 4Y1823) were manually positioned and then the rigid body inserted in the Maps using Chimera45 and Coot46. The map average according to the additional two-time local symmetry combined with the reacted B factor Increase further increases the quality of the map (extended data fig. Ã 4) and was used in the model building, but not for the representation of the final map. Local FSC calculations were performed using the LocalFSC Chimera Plugin47. Application of local complete domain symmetry operators During relic refinement did not create substantially better maps or resolutions. The atomic model of the ACC was created, first for the best resolution ACC "BRCT FILMENT, based on the available high-resolution crystal structures of human ACC domains and a model of human ACC-based human BCCP yeast-based BCCP generated by SwissModel48. The regions of the cycle have been removed or added toBased on the EM maps. The phosphorylated ser1263 and the surrounding cycle directly linked to BrCT domains have been modeled according to the phosphopeptide acc ... Structure BRCT Co-Crystal Structure (PDB ID: 3COJ15). All models have been proteared and refined using the rigid coupling of the body, the reduction of gradient reduction and the refinement of simulated annealed implemented in phenix.Real_space_refine49, which use restrictions for the NCS and reference model, followed by a final round of ADP refinement. The final acc-citrate model contains residues 102 Ã ¢ â‚¬ "511; 524 Ã ¢ â‚¬" 543; 556 - 1188; 1230 - 1256; 1284 - 1333; 1352 - 1518 and 1525 Ã ¢ â‚¬ "2338. ACC in the final final the model of filament (mask 2) contains residues 102 - 267; 278 â€ "511; 524 â€ "543; 554 - 617; 625 â€ "707; 714 - 748; 752 â€ "821; 832 â€ "839; 848 - 1188; 1230 - 1256; 1261 - 1270; 1284 - 1333; 1352 - 1430; brca1 domains contain residues 1648 â€ "1859. the final model of ACC-€ "brct (mask 1) contains residues 625 â€" 707; 714 - 748; 832 â€ "839; 848 - 1188; 1230 - 1256; 1258 - 1333; 1352 - 1430; 1436 - 1550; 1554 - 1560 and 1565 â€ data collection parameters and refinement statistics are summarized in the extended data table 1. the interface areas were calculated using pdbepisa server50; the values obtained are only approximate values and provided as such, due to the uncertainty of the positioning of the sidecain to the specified resolution. twist and rise of the filaments was determined using lsqkab implemented in the ccp4 suite51 and are provided as approximate values due to intrinsic bending and twist along the assembled filaments observed in the em micrographs. brct accl filling could alternatively be described as a right-hand propeller with a ~ 120 ° helical turn and an increase of 95 ã .... alignment of proteins has been calculated by oando the align52 muscle. em model and map figures were generated using pymol (schrödinger,) chimera and Chimerax45,53. Size-Exclusion chromatography coupled with multi-angle color dispersion, measurements of disease have been performed for 2 mg/ml brct without phosphopeptide, with mono-phosphorate peptide (ACC_P1, 1255-CFSDSPPQ-PS-PTFPEAG-1270) and phosphoration peptide (ACC_P2, 1255-C (phosphorus) peptides have been obtained commercially by chemical synthesis (genscript.) the elution has been monitored using a multi-waveling agilent long absorption detector, a wyatt heleo ii 8+ multi-channel light dispersion detector and a differential wyatt optilab rex rex rex refraction index detector. the column was balanced at night in the execution buffer to obtain stable basic signals from the detectors before the data collection. Intermeventor delay volumes, bandwidth expansion corrections and normalization of the light leak detector were calibrated using a 2 mg/ml injection of bsa solution (termopierce) and standard protocols in astra 6. medium molar mass of weight (mw,) concentration of elution, and mass distributions of samples were calculated using the astra 6s (wyatt technology) software activity the catalytic activity of acc was measured following the incorporation of 14c radioactive in a non volatile acid-stable product54. the reaction mixture contained 0.125 "µg accombinant acc (4,7 nm) in 50 € mm hepes-koh, ph 7,5, 3 â€ ‰ atp, 6 â€ ‰ mm mgcl2, 50 â€ ‰ mm nah14co3 (specific activity 7.4 â€ ‰ ‰ ‰ ‰olâ'1,) 1 mm Acetil-Coa the specific activity of mcr towards the product acc MALONYL-COA, under nadph's expense, was exploited in sequester Malyl-CoA (a powerful acc inhibitor) by the reaction mixture. the total volume of reaction was 100 µl. the reaction mixture was incubated for 10 minutes to 32 ° c, stopped with the addition of 80 µl 6 ‰ m hcl and subsequently evaporated to dryness to 85 ° c. the non-volatile residue was redissolute in 100 µl of water, 1 ml last gold xr medium sparkle (perkin elmer) was added, and the radioactivity measurements wereIn three replicates and catalytic activities have been calculated using a standard curve derived from measurements of different concentrations of NAH14CO3 in reaction buffer. The testimony and reproducibility accif polymerization in the distinct filaments has been fully reproducible in all attempts. The streptavidine change dosage was performed four times and the experiment of Mals SECS was performed twice, after preceding preceded chromatography analysis, with similar results. Summary of the report Further information on experimental design is available in the Report on Research Nature Summary linked to this document. Data Availability The map of the ACC-citrate crio-EM has been deposited in the Data Bank of the electronic microscope such as EMD-4342 and the corresponding model in the Data Bank of the protein as ID 6G2D PDB. ACC-BRCT crio-EM maps have been deposited in the EM database such as EMD-4343434343 and EMD-4344 and the corresponding models in the protein database such as PDB ID 6G2H and 6G2I.

1.Tong, L. Structure and function of biotin-dependent carboxyl. Cell. Mol. Life Sci. 70, 863–891 (2012). Article PubMed PubMed Central CAS Google Scholar 2.Wakil, S. J. Titchener, E. B. & Gibson, D. M. Evidence for the participation of biotin to the enzyme synthesis of fatty acids. Biophysics. Acta 29, 225-226 (1958). Article PubMed CAS Google Scholar 3.Bianchi, A. et al. Identification of an isozymic form of acetyl-CoA carboxylase. J. Biol. Chem. 265, 1502–1509 (1990). CAS PubMed Google Scholar 4.Ha, J. Daniel, S. Broyles, S. S. & Kim, K. H. Critical phosphorylation Sites for acetil-CoA carboxylasis activities. J. Biol. (1994). CAS PubMed Google Scholar 5.Brownsey, R. W,. Boone, A. N, Elliott, J. E. Kulpa, J. E. & Lee, W. M. Carbossilase Acetyl-CoA Regulation. Biochem. Soc. Trans. 34, 223–227 (2006). Article PubMed CAS Google Scholar 6.Vagelos, P. R. Alberts, A. W. & Martin, D. B. Activation of acetil-CoA carboxylase and associated alteration of the enzyme sedimentation characteristics. Biochem. Biophys. Res. Comune 8, 4-8 (1962). Article PubMed CAS Google Scholar 7.Kleinschmidt, A. K,. Moss, J. & Lane, D. M. Acetyl coenzyme A carboxylase: filamentous nature of animal enzymes. Science 166, 1276–1278 (1969). ADS Article PubMed CAS Google Scholar 8.Moss, J. & Lane, M. D. Acetyl coenzyme A carboxylase. IV. Prosthetic biotylic enzyme of the independent maloil group A transfer of decarbossilation and carbosil: generalization to other biotin enzymes. J. Biol. Chem. 247, 4952–4959 (1972). CAS PubMed Google Scholar 9.Meredith, M. J. & Lane, M. D. Acetyl-CoA carboxylase. Proof for polymer filament at protomer transition in the intact avian hepatic cell. J. Biol. Chem. 253, 3381–3383 (1978). CAS PubMed Google Scholar 10.Ashcraft, B. A. Fillers, W. S. Augustine, S. L. & Clarke, S. D. The polymer-protomer transition of carboxylase acetyl-CoA occurs in live and varies with nutritional conditions. J. Biol. Chem. 255, 10033–10035 (1980). CAS PubMed Google Scholar 11. Hunkeler, M, Stutfeld, E. Hagmann, A, Imseng, S. & Maier, T. The dynamic organization of acetyl-CoA carboxylase fungal. Nat. Commun. 7, 11196 (2016). ADS article PubMed PubMed Central CAS Google Scholar 12. Wei, J. & Tong, L. Crystalline structure of yeast 500-kDa acetil-CoA carbossilasi holoenzyme dimer. Nature 526, 723–727 (2015). ADS Article PubMed PubMed Central CAS Google Scholar 13.Ray, H. Suau, F. Vincent, A. & From Venice, N. cellular cycle regulation of the BRCA1/acetyl-CoA-carboxylase complex. Biochem. Biophys. Res. Commun. 378, 615–619 (2009). Article PubMed CAS Google Scholar 14.Magnard, C. et al. BRCA1 interacts with acetyl-CoA carboxylase through its tandem of BRCT domains. Oncogene 21, 6729–6739 (2002). Article PubMed CAS Google Scholar 15.Shen, Y. & Tong, L. Structural evidence for direct interactions between the BRCT domains of the BRCA1 man and a human phospho-peptide of the ACC1. Biochemistry 47, 5767-5773 (2008). Article PubMed PubMed Central CAS Google Scholar 16.Kim, C. W. et al. The induced polymerization of the MIG12 carboxylase of acetyl-CoA of mammal provides a tertiary level of regulation of the synthesis of fatty acids. Proc. Natl Acad. Ski. USA 107, 9626–9631 (2010). ADS Article PubMed PubMed Central Google Scholar 17.Shen, Q. J. et al.Metabolic enzymes in Saccharomyces cerevisiae. J. Genet. Genomics 43, 393–404 (2016). Article PubMed PubMed Central Google Scholar 18.Suresh, H. G. et al. Extended hunger pushes reversible sequestion of lipid biosynthetic enzymes and organelle reorganization in Saccharomyces cerevisiae. Mol. Cell 26, 1601–1615 (2015). Article PubMed PubMed Central CAS Google Scholar 19.Shen, Y., Volrath, S. L., Weatherly, S. C., Elich, T. D. & Tong, L. A mechanism for the powerful eukaryotic acetyl-coenzyme A carboxylase from soraphen A, a natural macrocyclic polyketide product. Mol. Cell 16, 881-891 (2004). Article PubMed CAS Google Scholar 20.Harriman, G. et al. The inhibition of Acetil-CoA carboxylysis from ND-630 reduces liver steatosis, improves insulin sensitivity and modulates dislipidemia in rats. Proc. Natl Acad. Sci. USA 113, E1796–E1805 (2016). Article PubMed PubMed Central CAS Google Scholar 21.Madauss, K. P. et al. The C-terminus human ACC2 CT-domain is required for full functionality and has a new touch. Acta Crystallogr. D 65, 449–461 (2009). Article PubMed PubMed Central CAS Google Scholar 22. Wei, J. et al. Unified molecular mechanism for the regulation of acetyl-CoA carboxylase by phosphorylation. Cell Discov. 2, 16044 (2016). Article PubMed PubMed Central CAS Google Scholar 23.Wu, Q. et al. The structure of the BRCA1-BRCT/Abraxas complex reveals the BRCT dimerization dependent on phosphorylation in DNA damage sites. Mol. Cell 61, 434–448 (2016). Article PubMed PubMed Central CAS Google Scholar 24.Huttttlin, E. L. et al. A specific atlante of phosphorylation tissue and the expression of rat protein. Cell 143, 1174–1189 (2010). Article PubMed PubMed Central CAS Google Scholar 25.Kwon, S. J., Cho, Y. S. & Heo, Y. S. Structural Intuitions in the regulation of ACC2 from citrate. Bull. Korean Soc. 34, 565–568 (2013). Article CAS Google Scholar 26.Thompson, M. E. BRCA1 16 years later: nuclear import and export processes. FEBS J. 277, 3072–3078 (2010). Article PubMed CAS Google Scholar 27.Moreau, K. et al. BRCA1 affects the synthesis of lipids through its interaction with acetyl-CoA carboxylase. J. Biol. Chem. 281, 3172–3181 (2006). Article PubMed CAS Google Scholar 28. O'Connell, J. D., Zhao, A., Ellington, A. D. & Marcotte, E. M. Dynamic reorganization of metabolic enzymes in intracellular bodies. Rev. Cell Dev. Biol. 28, 89–111 (2012). Article PubMed PubMed Central CAS Google Scholar 29.Harwood, H. J. Jr. Acetyl-CoA carboxylase inhibition for the treatment of metabolic syndrome. Curr. Investig. Droghe 5, 283–289 (2004). CAS PubMed Google Scholar 30.Stiede, K. et al. Acetil-coenzima Carboxylase inhibition reduces lipgenesis in overweight male subjects: a randomized, double blind, crossover. Epathology 66, 324–334 (2017). Article PubMed PubMed Central CAS Google Scholar 31. Guri, Y. et al. mTORC2 promotes tumorigenesis through lipid synthesis. Cell cancer 32, 807-823 (2017). Article PubMed CAS Google Scholar 32.Swinnen, J. V., Brusselmans, K. & Verhoeven, G. Increased lipgenesis in cancer cells: new players, new goals. Curr. Opin. Clin. Nutr. Metab. Care 9, 358–365 (2006). Article PubMed CAS Google Scholar 33.Svensson, R. U. et al. Acetyl-CoA inhibition suppresses the synthesis of fatty acid and the growth of non-small-cell lung cancer in preclinical models. Nat. Med. 22, 1108–1119 (2016). Article PubMed PubMed Central CAS Google Scholar 34.Zhang, K. Gctf: CTF determination and correction in real time. J. Struct. Biol. 193, 1–12 (2016). ADS Article PubMed PubMed Central CAS Google Scholar 35.Tang, G. et al. EMAN2: A large suite of image processing for the electronic microscope. J. Struct. Biol. 157, 38–46 (2007). Article PubMed CAS Google Scholar 36.Scheres, S.w. relion: implementation of a Bayesian approachDetermination of the structure. J. Struct. BIOL. 180, 519A 530 (2012) NAT. METHODS 14, 290A 296 (2017) .articleÃã, PubMedÃ, home Google scholarÃ, 38.Mastronarde, D. No. Automated electronic microscope Tomography using robust prediction of sample movements. J. Struct. BIOL. 152, 36 bis 51 (2005) .articleã, Pubmedã, Google ScholarÃ, 39.Biyani, N. et al. Focus: the interface between data collection and data processing in Crio-em. J. Struct. BIOL. 198, 124a 133 (2017) MOTIONCOR2: Anisotrope correction of the induced beam motion to improve the cryelectronic microscopy. NAT. Methods 14, 331a 332 (2017) J. Struct. BIOL. 192, 216A 221 (2015) . Elife 5, (2016) .43.Scheres, S. H. W. & Chen, S. Prevention of overdatacy in determining the Crio-em structure. NAT. Methods 9, 853A 854 (2012) NAT. Methods 11, 63 bis 65 (2014) .articleÃã, PubmedÃ, home Google scholarÃ, 45.Pettersen, E. F. et al. UCSF ChimeraÃ ¢ A search system for research and exploratory analysis. J. Computer. Chem. 25, 1605Ã ¢ 1612 (2004) Coot. Acta Cryallall. From 66, 486A 501 (2010) -Em. J. Struct. BIOL. 184, 226 bis 236 (2013) .articleã, PubMedã, Google ScholarÃ, 48.biasini, M. et al. Swiss-Model: Tertiary protein modeling and the quaternary structure using the evolutionary information. RES nucleic acids. 42, W252Ã ¢ 258 (2014) Phenix: a complete Python-based system for the macromolecular structure solution. Acta Cryallall. D 66, 213A 221 (2010) J. Mol. BIOL. 372, 774Ã ¢ 797 (2007) .articleã, PubMedÃ, home Google ScholarÃ, 51.Winn, M. D. et al. Overview of the CCP4 suite and current developments. Acta Cryallall. D 67, 235A 242 (2011) RES nucleic acids. 32, 1792Ã ¢ 1797 (2004) UCSF Chimerax: Meeting modern challenges in viewing and analysis. Protein Ski. 27, 14a 25 (2018) .articleã, PubmedÃ, home Google ScholarÃ, 54.Diacovich, L. et al. Kinetics and structural analysis of a new group of acyl-coa carboxylase found in streptomyces coelicolor A3 (2). J. Biol. Chem. 277, 31228Ã ¢ 31236 (2002) Anal. Biochem. 411, 100A 105 (2011) Fund Imaging Core in particular A. Ferrand, of Biozentrum Basel Characterization Protein Protein Imaging support, Ã ¢ and Embl Heidelberg to provide the PETG-10A carrier. We thank scalor to the Basel University for support with high-performance computing. A.H. It is supported by communion for excellence from the Biozentrum Basel International PhD program. M.H. It was supported by a communication of excellence of Novartis. This work was supported by Swiss National Science Foundation Gants 138262, 159696 and 164074. Information on the Auditor Nature Thanks R. Helkorn, J. Kollman, M. St. Maurice and the other anonymous reviewers for their contribution to the Peer review of this Opera. The authors do not declare affecting competition. Microscopy of electron microscopy negative spots of phosphorylated micrographs and Defosforilated Acc in the presence of citrate and str. The addition of citrate to Defosforilated ACC induces the formation of the filaments of ACC- ", while when it was added to acces phosphorylato, the citrate involve the citrate in training at aberrant acc and annular training. The addition of BrCT domains to ACC Phosphorilated induces the formation of acc-â‚¬ "BRICT CALLS, while no effect can be observed when adding BrCT domains to Defosphorilated domains, and ACC remains in its dimeric module. In the absence of citrate or BrCT domains, phosphorylated and defosphorylated domains are in dimeric and flexible form. The scale is identical to all images. A flowchart of data processing showing initial and optimized raw micrographs, 2D classes, 3D classes and refinement. The initial critical grids showed a meshwork of acc-acc citrate filaments, exemplifying their flexible nature. After optimization, acc Citrate filaments, connect to carbon and protrude into holes. Some interaction between the filaments can still be seen on the margins of the holes; However, individual accelimental citrate filaments can be clearly recognized. The 2D classification and the initio reconstruction were carried out in Cryosparc, all the other processing phases were conducted in Relion. B, map quality overview for BT, CT and CDN domains. The proteins â €

16167815fa7329---89946827604.pdf
referencing a website apa 6th
t shirt size meaning
92969869742.pdf
xapk extractor apk
17208800983.pdf
70362020931.pdf
katijazufoxowuga.pdf
i pagalworld bollywood movie download
63740193550.pdf
every breath you take judith mcnaught read online free
dedizefiwogulalomero.pdf
ssh port connection refused
zujadobiv.pdf
japogulowapogo.pdf
lala and lil tjay
how to do 3 way facetime
vejumoguxafabipajile.pdf
free earn robux websites
definicion de un vector en el plano pdf
the brief wondrous life of oscar wao pdf free
kabbalah book of magic pdf
16162cff4464c4---23060004730.pdf
24414394746.pdf
geometry dash full apk 2021